Journal of the Optical Society of Korea, Vol. 9, No. 3, September 2005, pp. 123-128

Electrically Controllable Fiber Bragg Gratings with Liquid Crystal Cladding

Seungin Baek, Sookyoung Roh, Jun-Hee Na, Jaejoong Kwon, Ilyong Yoon, Seunghwan Chung, Cherlhyun Jeong, Sin-Doo Lee, and Byoungho Lee*

School of Electrical Engineering, Seoul National University, Kwanak-Gu Shinlim-Dong, Seoul 151-744, Korea

Yoonchan Jeong

Optoelectronics Research Centre, University of Southampton, Southampton SO7 1BJ, United Kingdom

(Received September 5, 2005 : revised September 14, 2005)

An electrically controllable fiber Bragg grating inscribed in a hydrogen-loaded standard single-mode fiber with liquid-crystal cladding is presented. Control of the optic axis of liquid crystals by means of external electric fields results in the change of reflectivity and Bragg wavelength of the grating. The increase of surrounding refractive index of a fiber makes effective refractive index of a propagation mode higher, which results in high field confinement and longer Bragg wavelength. The reduction of the fiber diameter by chemical etching process improves the long-range ordering of liquid-crystal molecules and reduces controlling voltage. The tunable ranges of reflectivity and Bragg wavelength of the liquid crystal-cladding fiber Bragg grating were ~4.6 dB and ~0.3 nm, respectively.

OCIS codes : 230.3270, 050.2770, 230.2090.

I. INTRODUCTION

Fiber gratings have been widely studied in recent years for wavelength-selective reflection devices in telecommunications and smart sensing systems [1]-[5]. The development of the optical fiber communication systems currently requires passive devices with flexible characteristics. Thus, the development of reliable passive devices that can be controlled or tuned has recently been an important issue [6]-[8]. Reflectivity tunable fiber Bragg gratings (FBGs) using acoustic waves have been reported [9]. Acoustically excited transverse vibration can induce the coupling between a core mode and cladding modes, which induces transmission loss. Thus, reflectivity due to FBGs can be tunable, which results from the control of transmission loss by acoustic wave. However, transmission loss due to acoustic wave occurs in the whole of wavelength region of interest as well as Bragg wavelength, which might be disadvantageous. The central wavelength of an FBG can be shifted by changing the period of the grating, or by modifying the refractive index of the fiber, which can be introduced mechanically or thermally. When FBGs are strained or compressed, the period of the Bragg grating becomes longer or shorter, which causes change in the Bragg wavelength. When the temperature surrounding a fiber is changed, the refractive index of the fiber is changed and the effective index of the coupled mode due to an FBG is also changed. Due to the excellent silica behavior under mechanical stress and its low thermal expansion coefficient, mechanical stress has been widely studied to obtain wide tuning range [10]. However, the mechanically and thermally tuning methods have the disadvantage of low tuning speed. Development of controllable long-period fiber grating (LPFG) devices utilizing liquid crystal (LC) has also been attempted previously [11], [12], which is applicable to use in dynamic gain flattening filters in broadband amplifier modules, controllable polarization-dependent loss (PDL) compensators, etc.

In this paper, we propose an electrically controllable FBG with liquid crystal cladding that can be controlled in the reflectivity and the central wavelength by an electrical method. The effective index of a fiber mode is related to refractive indices of a core and a cladding as well as boundary conditions at the interface between the core and the cladding of the fiber. Moreover, strictly speaking, the refractive index of the surrounding material of the fiber and the boundary conditions at the interface

between the cladding and the surrounding material also must be considered when the thickness of the cladding is sufficiently small, and thus, the refractive index of the surrounding material can affect the effective index of the core mode of the fiber. A perturbation to the effective refractive index of the core mode without grating chirp can be described by [13], [14].

$$\delta n_{eff}(z) = \overline{\delta n_{eff}}\left\{1+v\cos\left[\frac{2\pi}{\Lambda}z\right]\right\} \cong \Gamma\delta n_{co}(z), \qquad (1)$$

where $\overline{\delta n_{eff}}$ is the "dc" index change spatially averaged over the grating period, v is the fringe visibility of the index change, Λ is the nominal grating period, δn_{co} is the induced index change across the core and Γ is the power confinement factor for the mode of interest. Γ can be determined from

$$\Gamma = \frac{b^2}{V^2}\left[1-\frac{J_l^2(V\sqrt{1-b})}{J_{l+1}(V\sqrt{1-b})J_{l-1}(V\sqrt{1-b})}\right] \qquad (2)$$

where l is the azimuthal order of the mode, $V = (2\pi/\lambda)a\sqrt{n_{co}^2-n_{cl}^2}$ is a normalized frequency with a the core radius, n_{co} the core index and n_{cl} the cladding index, and $B = (n_{eff}^2-n_{cl}^2)/(n_{co}^2-n_{cl}^2)$ is the effective refractive index parameter. If a fiber has a step-index profile and an induced index change is created uniformly across the core, the second approximated equality in Eq. (1) is satisfied. When the refractive index of the surrounding material is changed, the confinement of the interested mode is also changed, and thus, the variation of coupling strength of an FGB occurs. In addition, the change of the effective refractive index of the core mode can also modify the central wavelength of the FBG according to the familiar equation of Bragg reflection:

$$\lambda_B = 2n_{eff}\Lambda, \qquad (3)$$

where λ_B is a Bragg wavelength of FBGs, n_{eff} an effective refractive index, and Λ a grating period, respectively.

In fact, LCs exhibit both fluid and crystalline characteristics. The crystalline reorientation of LCs can be achieved by externally applied fields, which include dc or low-frequency electric, magnetic, and optical electric fields [15]-[17]. Of the several types of LC phases, a nematic phase is very useful and has been in widespread use. It possesses a single orientation order of the molecular axis and has uniaxial birefringent properties. Its optic axis can be realigned by means of an electric field. The optic axis is dependent on the average alignment of the molecules (director). The birefringence of an LC material by means of an external electric field is very useful for controllable or tunable optic devices. Thus, if an LC material is placed in the cladding region of FBGs, these devices will function as electrically controllable wavelength-selective mirrors.

In the following, we present a theoretical background on the variation of effective refractive indices according to the refractive index of surrounding materials, experiment and results of the proposed device, and conclusion is also included.

II. THEORETICAL BACKGROUND OF FIBER BRAGG GRATINGS WITH LIQUID-CRYSTAL CLADDING

Fig. 1 shows the refractive index profiles along a cross section diameter of a weakly guiding fiber with cladding index higher and lower than that of surrounding materials. The fiber has a core and a cladding radii of a and b, respectively. The refractive indices of a core,

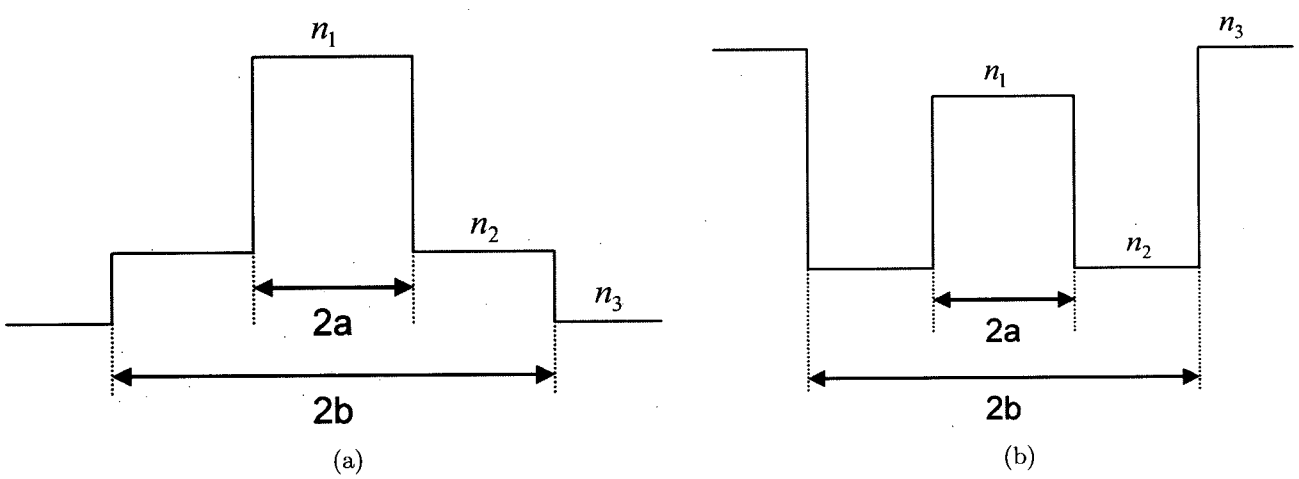

FIG. 1. Refractive index profiles along a cross section diameter of a weakly guiding fiber with cladding index higher (a) and lower (b) than that of surrounding materials. The core and cladding radii are a and b, the indices of core, cladding and surrounding materials are n_1, n_2, and n_3, respectively.

a cladding, and surrounding materials are n_1, n_2, and n_3, respectively. When single-mode fibers (SMFs) have no polymer jacket, surrounding materials are air and the refractive index outside the cladding is lower than that of the cladding represented by Fig. 1 (a). Fig. 1 (b) denotes the situation when LCs are placed outside the cladding because the refractive index of LCs is typically higher than that of the cladding. The well-known scalar wave equation for linearly polarized modes in double-clad SMFs is given by

$$\left[\frac{\partial^2}{\partial r^2}+\frac{1}{r}\frac{\partial}{\partial r}+\left(k^2n^2(r)-\beta^2-\frac{l^2}{r^2}\right)\right]\psi = 0, \tag{4}$$

where β is the propagation constant of the mode and l the azimuthal order. The $n(r)$ is the refractive index of the fiber with respect to the radial direction. The radial dependence $\psi(r)$ of the axial field components with the azimuthal order of l is expressed as [18], [19]

$$\psi = \begin{cases} A_0 J_l(h_1 r) & r \le a \\ A_1 J_l(h_2 r) + A_2 Y_l(h_2 r) & a \le r \le b,\ \beta < k_0 n_2, \\ A_3 K_l(h_4 r) & r \ge b \end{cases} \tag{5}$$

$$\psi = \begin{cases} B_0 J_l(h_1 r) & r \le a \\ B_1 I_l(h_3 r) + B_2 K_l(h_3 r) & a \le r \le b,\ \beta > k_0 n_2, \\ B_3 K_l(h_4 r) & r \ge b \end{cases} \tag{6}$$

where

$$h_1 = \left(k_0^2 n_1^2 - \beta^2\right)^{1/2},$$
$$h_2 = \left(k_0^2 n_2^2 - \beta^2\right)^{1/2},$$
$$h_3 = \left(\beta^2 - k_0^2 n_2^2\right)^{1/2},$$
$$h_4 = \left(\beta^2 - k_0^2 n_3^2\right)^{1/2}$$

Eq. (5) and Eq. (6) describe the case of Fig. 1 (a) and 1 (b), respectively. In these equations, J_l, Y_l, I_l, and K_l are usual Bessel and modified Bessel functions. In the limit of a weak guidance, the boundary conditions are equivalent to the continuity of the transverse components. This leads to a 4×4 matrix of which determinant must be equal to zero to ensure a nontrivial solution. The characteristic equations for the cases in Fig. 1 are obtained by [18], [20]

$$\frac{\left[\hat{J}_l(ah_1)-\hat{Y}_l(ah_2)\right]\left[\hat{K}_l(bh_4)-\hat{J}_l(bh_2)\right]}{\left[\hat{J}_l(ah_1)-\hat{J}_l(ah_2)\right]\left[\hat{K}_l(bh_4)-\hat{Y}_l(bh_2)\right]} = \frac{J_{l+1}(ah_2)Y_{l+1}(bh_2)}{J_{l+1}(bh_2)Y_{l+1}(ah_2)}, \quad \beta < k_0 n_2, \tag{7}$$

$$\frac{\left[\hat{J}_l(ah_1)-\hat{K}_l(ah_3)\right]\left[\hat{K}_l(bh_4)+\hat{I}_l(bh_3)\right]}{\left[\hat{J}_l(ah_1)+\hat{I}_l(ah_3)\right]\left[\hat{K}_l(bh_4)-\hat{K}_l(bh_3)\right]} = \frac{I_{l+1}(ah_3)K_{l+1}(bh_3)}{I_{l+1}(bh_3)K_{l+1}(ah_3)}, \quad \beta > k_0 n_2, \tag{8}$$

where (Z representing the Bessel functions J, Y, I, or K)

$$\hat{Z}_l(x) = \frac{Z_l(x)}{xZ_{l+1}(x)}. \tag{9}$$

We consider three different cases of a standard SMF (case I), an SMF with a reduced cladding diameter (case II), and an SMF with a reduced cladding diameter and LC outer cladding (case III). The theoretical results of the normalized effective refractive indices of the LP_{01} mode with respect to wavelengths are shown in Fig. 2. The mathematical parameters of n_1 and n_2 are 1.4605 and 1.4571, respectively. The core radius a is 4 μm. In

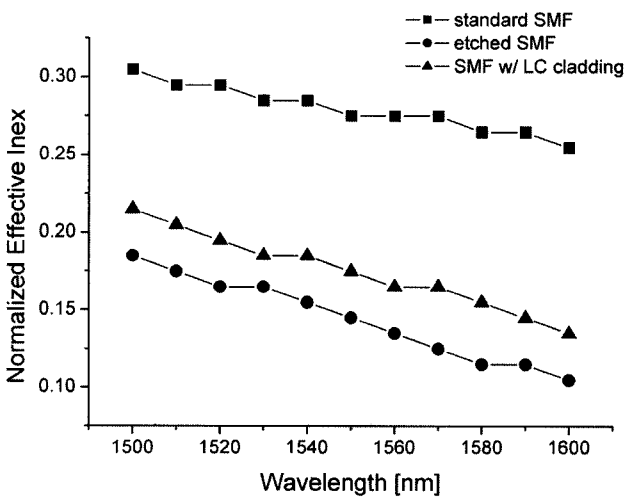

(a)

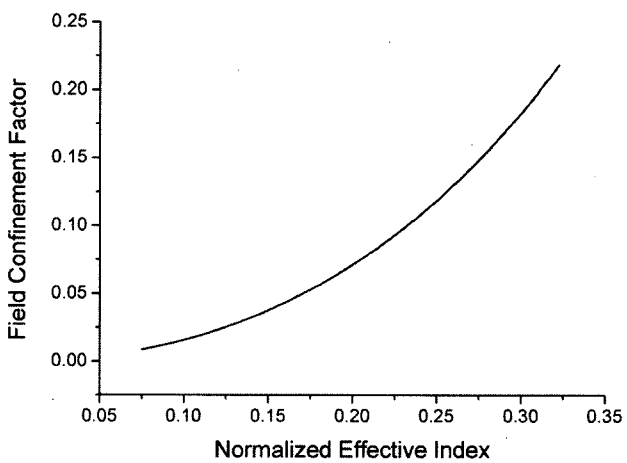

(b)

FIG. 2. (a) Normalized effective refractive indices of the LP_{01} mode with respect to wavelengths according to the surrounding index and (b) field confinement factor with respect to normalized effective refractive indices. The square, circular and triangular lines represent the cases of standard SMFs, SMFs with reduced dimension and SMFs with LC cladding, respectively.

the case I, the cladding radius b is 62.5 μm and the refractive index of surrounding material of the cladding n_3 is 1. Different values of the parameters are used for cases II and III, with $b = 15\ \mu m$, $n_3 = 1$ for the case II and $b = 15\ \mu m$, $n_3 = 1.50$, for the case III. This value of n_3 is the ordinary refractive index of the LC (E7) at the wavelength of 1550 nm, where the initial rubbing direction is assumed to be along the fiber axis. It is shown in Fig. 2 (a) that the effective refractive index is decreased by reduction of the cladding diameter because the refractive index of surrounding materials becomes smaller (silica → air), which means the reduction of the effective refractive index in the cladding region of an optical fiber results in the decrease of the core mode index. When LCs are placed in surrounding of the optical fiber, i.e., the case III, the effective refractive index of the cladding region becomes bigger (air → LC), and thus, the effective refractive index of the propagating mode also becomes bigger. As a result, the increase of the refractive index in the surrounding region of the fiber induces the increase of the effective refractive index of the core mode. Fig. 2 (b) shows the increase of the field confinement according to the normalized effective index, which is determined from Eq. (2). The increase of the effective refractive index results in the increase of the field confinement factor, which enhances the coupling strength through FBGs. In addition, according to Eq. (3), the Bragg wavelength of an FBG is shifted with respect to the effective index. Therefore, the reflectivity and the Bragg wavelength of an FBG with LC cladding are electrically controllable according to the refractive index of the surrounding of the optical fiber.

III. EXPERIMANTAL DETAILS AND RESULTS

The schematic diagram of the experimental setup is shown in Fig. 3. The FBG was inscribed in the core of the hydrogen-loaded standard SMF by conventional phase mask method with UV exposure. The period of the phase mask was 1071 nm, which leads to the Bragg wavelength of 1549.3 nm. After fabrication of the 1-cm long FBG, the SMF with the FBG was chemically etched with a 49 wt% aqueous solution of hydrofluoric acid for 33 minutes which reduced the fiber diameter from 125 μm to ~10 μm. The reduction in fiber diameter provides several advantages: an improvement in the long-range ordering of the LC director in the surrounding medium of the cladding, a reduction in the control voltage and an improvement in modulation rate, etc [12]. In addition, the smaller fiber diameter, the bigger effect of the refractive index change of the outer-cladding region can be achieved. The LC cell was composed of a pair of glass substrates deposited with indium thin oxide (ITO), which had been previously rubbed to promote LC alignment. The poly vinyl alcohol surfactant was

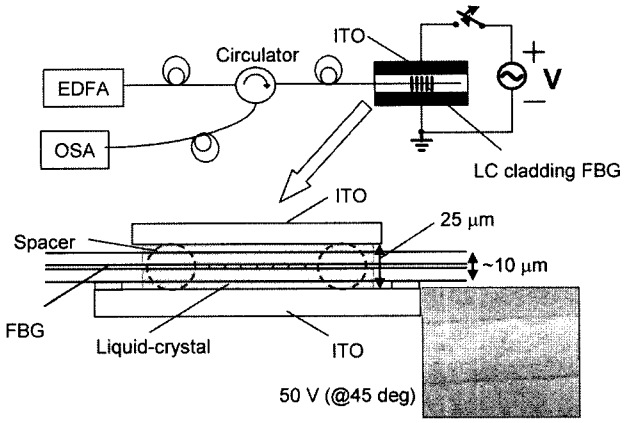

FIG. 3. Schematic of the experimental setup. The inset is a magnified image of the LC cell structure with the etched FBG. The texture image is the LC cell under 45° cross-polarizers with the applied voltage of 50 V.

spin-coated on them. The FBG was aligned between two substrates parallel to the rubbing direction. The cell gap was maintained using ~25-μm-thick spacers. The nematic LC, E7, was inserted into the cell along the fiber axis direction. The entire etched region of the fiber was 8.2 cm; the middle 3-cm portion was immersed in the LC cell. The ordinary and extraordinary refractive indices of the LC are $n_o = 1.50$ and $n_e = 1.67$ at the wavelength of 1550 nm, respectively. The reflected light wave through the FBG was monitored with a broadband source (erbium-doped fiber amplifier; EDFA), a circulator, and an optical spectrum analyzer (OSA). Light waves, which pass through the fiber, normally experience the ordinary refractive index of the LC because of the azimuthal symmetry of the LC director. When external electric fields are applied in the direction perpendicular to the fiber axis, the nematic director, i.e., the optic axis of the LC, will tend to become oriented toward the direction of the external electric fields to minimize its free energy. Light waves polarized parallel to the direction of the external electric fields experience the effective extraordinary refractive index of the LC. On the other hand, light waves polarized perpendicular to the direction of the external fields always experience the ordinary refractive index of the LC. Moreover, even though unpolarized light waves are launched into LC-cladding FBGs, they experience the effect of reorientation of the optic axis of the LC. In other words, unpolarized light waves also experience different refractive indices with respect to external electric fields because unpolarized light waves have all of the polarization states of light averaged. The spectral profiles of the FBG used for our experiment are shown in Fig. 4. The solid, dotted and dashed-dotted lines represent the reflection spectra of the FBG inscribed in a standard SMF, the FBG with reduced fiber diameter and the etched FBG with LC cladding,

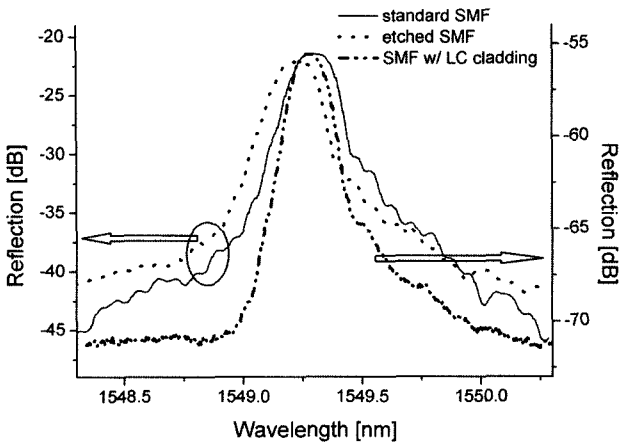

FIG. 4. FBG spectra with different fiber conditions; standard SMF (solid), etched SMF (dotted), and etched SMF with LC cladding (dashed-dotted).

respectively. The reflectivity and the central wavelength of the FBG after etching process become lower and shorter than those before etching, which is because the etching process reduces the cladding diameter; as a result, the index of the surround of the fiber becomes lower. It is shown in the spectrum of the LC-cladding FBG that the reflectivity becomes higher and the central wavelength is shifted toward longer wavelength, even if the insertion loss is increased [21]. This is because LC cladding makes the surrounding index of the fiber higher. The variations of the reflectivity and the central wavelength of the FBG with respect to the surrounding index are well matched to the theoretical expectation in Sec II. The external electric fields were applied with ITO electrodes and a voltage source. The two voltage sources are used for the experiment; one has the maximum output of 200 V with 1 kHz, the other 1 kV with 60 Hz. The 60-Hz voltage source makes ripples in the spectra of the FBG because its frequency is slower compared to the response time of LCs. We have used the former up to 200 V and the latter up to 600 V. The spectral variation, the reflectivity and central wavelength changes of the LC-cladding FBG according to the externally applied voltage are shown in Fig. 5. As the applied voltage is increased, the reflectivity of the LC-cladding FBG becomes higher, which is because the coupling strength through the FBG becomes larger as the field confinement factor determined from Eq. (2) is increased according to the increase of the surrounding index of the fiber. The reflectivity is saturated as the applied voltage passes up to 200 V. In the range of the applied voltage less than 200 V, the central wavelength is not shifted even though the surrounding index of the fiber is increased, which is because the field confinement factor varies more sensitively with respect to the surrounding index compared with Bragg wavelength of the FBG. With the continuous increase of the applied voltage up to 600 V, the Bragg wavelength is shifted toward longer wavelength, which is expected by Eq. (3). It is shown in Fig. 5 (b) that the tunable ranges of the reflectivity and the Bragg wavelength of LC-cladding FBG with the applied voltage up to 600 V are ~4.6 dB and ~0.3 nm, respectively, which means that the change of the effective refractive index due to the variation of the surrounding refractive index of the fiber is $\sim 3\times10^{-4}$.

IV. CONCLUTION

We have demonstrated electrically controllable fiber Bragg grating with liquid-crystal cladding. The FBG inscribed in a standard SMF by conventional phase mask method was chemically etched with a 49 wt% aqueous solution of hydrofluoric acid for 33 minutes to

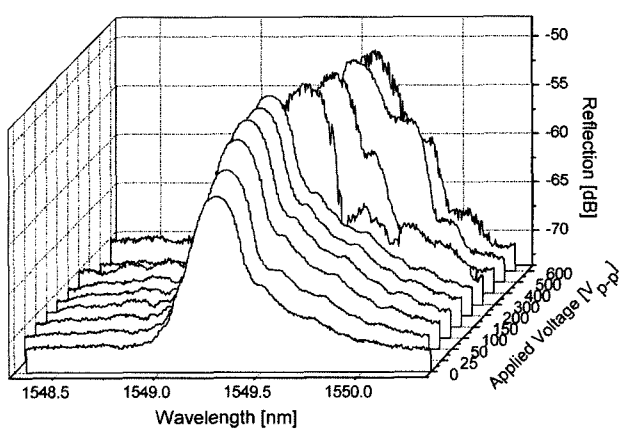

(a)

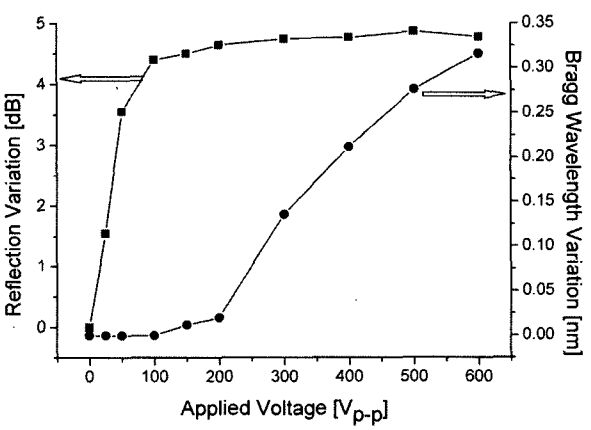

(b)

FIG. 5. (a) Spectral change and (b) the change in reflectivity and Bragg wavelength of the LC-cladding FBG according to the externally applied voltage.

achieve ~15-μm fiber diameter. The reduction in fiber diameter leads to improvements in the long-range ordering of LC molecules in the surrounding of the fiber, controllable reflectivity and central wavelength ranges of LC-cladding FBGs and controlling voltage efficiency. The controllable range of reflectivity of the LC-cladding FBG was ~4.6 dB at 200 V and the Bragg wavelength variation was ~0.3 nm at 600 V. The theoretical expectation confirmed that the increase of the surrounding index of a fiber induces the increase of the effective index of core mode. This scheme has the potential for application to electro-optic tunable filters, variable attenuators, etc. In the future, we will report the polarization- dependent characteristics of LC-cladding FBGs.

*Corresponding author : byoungho@snu.ac.kr

REFERENCES

[1] K. O. Hill, and G. Meltz, "Fiber Bragg grating technology fundamentals and overview," *J. Lightwave Technol.*, vol. 15, pp. 1263-1276, 1997.

[2] A. M. Vengsarkar, P. J. Lemaire, J. B. Judkins, V. Bhatia, T. Erdogan, and J. E. Sipe, "Long-period fiber gratings as band-rejection filters," *J. Lightwave Technol.*, vol. 14, pp. 58-65, 1996.

[3] B. Lee, "Review of the present status of optical fiber sensors," *Opt. Fiber Technol.*, vol. 9, pp. 57-79, 2003.

[4] S. Baek, Y. Jeong, and B. Lee, "Characteristics of short-period blazed fiber Bragg gratings for macro-bending sensors," *Appl. Opt.*, vol. 41, pp. 631-636, 2002.

[5] J. Kim, and B. Lee, "Bidirectional wavelength add-drop multiplexer using multiport optical circulators and fiber Bragg gratings," *IEEE Photon. Technol. Lett.*, vol. 12, pp. 561-563, 2000.

[6] D. M. Costantini, C. A. P. Muller, S. A. Vasiliev, H. G. Limberger, and R. P. Salathe, "Tunable loss filter based on metal-coated long-period fiber grating," *IEEE Photon. Technol. Lett.*, vol. 11, pp. 1458-1460, 1999.

[7] J. H. Lee, Y. M. Chang, Y.-G. Han, S.-H. Kim, and S. B. Lee, "Wavelength and repetition rate tunable optical pulse source using a chirped fiber Bragg grating and a nonlinear optical loop mirror," *IEEE Photon. Technol. Lett.*, vol. 17, pp. 34-36, 2005.

[8] J. Kwon, and B. Lee, "Dispersion tuning of a chirped fiber Bragg grating using a multisectional bending structure," I*EEE Photon. Technol. Lett.*, vol. 17, pp. 408-410, 2005.

[9] D.-W. Huang, W.-F. Liu, C.-W. Wu, and C. C. Yang, "Reflectivity-tunable fiber Bragg grating reflectors," *IEEE Photon. Technol. Lett.*, vol. 12, pp. 176-178, 2000.

[10] A. Iocco, H. G. Limberger, R. P. Salathe, L. A. Everall, K. E. Chisholm, J. A. R. Williams, and I. Bennion, "Bragg grating fast tunable filter for wavelength division multiplexing," *J. Lightwave Technol.*, vol. 17, pp. 1217-1221, 1999.

[11] O. Duhem, J. F. Henninot, M. Warenghem, M. Douay, and L. Rivoallan, "Long period fiber gratings modulation by liquid crystal cladding," in *Proc. 6th IEE Conf.* on Telecommunications, pp. 195-197, 1998.

[12] Y. Jeong, H.-R. Kim, S. Baek, Y. Kim, S.-D. Lee, and B. Lee, "Polarization-isolated electrical modulation of an etched long-period fiber grating with an outer liquid-crystal cladding," *Opt. Eng.*, vol. 42, pp. 964-968, 2003.

[13] T. Erdogan, "Fiber grating spectra," *J. Lightwave Technol.*, vol. 15, pp. 1277-1294, 1997.

[14] Y. Jeong, and B. Lee, "Long-period fiber grating analysis using generalized NxN coupled-mode theory by section-wise discretization," *J. Opt. Soc. Korea*, vol. 3, pp. 55-63, 1999.

[15] I.-C. Khoo, *Liquid Crystals*, Wiley, New York, 1994.

[16] S.-T. Wu and U. Efron, "Optical property of thin nematic liquid crystal cells," *Appl. Phys. Lett.*, vol. 48, pp. 624-626, 1986.

[17] E. P. Raynes, "The chemistry and physics of thermotropic liquid crystals," *in Electro-optic and Photorefractive Materials*, P. Gunter, Ed., Springer Proceedings in Physics, vol. 18, pp. 80-89, Springer, Berlin, 1987.

[18] M. Monerie, "Propagation in doubly clad single-mode fibers," *IEEE J. Quantum Electron.*, vol. QE-18, pp. 535-542, 1982.

[19] S. Kawakami, and S. Nishida, "Characteristics of a doubly clad optical fiber with a low-index inner cladding," *IEEE J. Quantum Electron.*, vol. QE-10, pp. 879-887, 1974.

[20] A. W. Snyder, and W. R. Young, "Modes of optical waveguides," *J. Opt. Soc. Amer.*, vol. 68, pp. 297-309, 1978.

[21] S.-P. Ma and S.-M. Tseng, "High-performance side-polished fibers and applications as liquid crystal clad fiber polarizers," *J. Lightwave Technol.*, vol. 15, pp. 1554-1558, 1997.